Self-adaptive low friction coatings based on transition metal dichalcogenides

Tomas Polcar, Albano Cavaleiro

PII: S0040-6090(11)00230-6
DOI: doi: 10.1016/j.tsf.2011.01.180
Reference: TSF 28709

To appear in: *Thin Solid Films*

Received date: 4 June 2010
Revised date: 12 October 2010
Accepted date: 5 January 2011

Please cite this article as: Tomas Polcar, Albano Cavaleiro, Self-adaptive low friction coatings based on transition metal dichalcogenides, *Thin Solid Films* (2011), doi: 10.1016/j.tsf.2011.01.180

Self-adaptive low friction coatings based on transition metal dichalcogenides

Tomas Polcar[1,2,*] and Albano Cavaleiro[2]

1) Department of Control Engineering, Faculty of Electrical Engineering, Czech Technical University in Prague, Technická 2, Prague 6, Czech Republic
2) SEG-CEMUC - Department of Mechanical Engineering, University of Coimbra, Rua Luís Reis Santos, P-3030 788 Coimbra, Portugal
*) contact: polcar@fel.cvut.cz

This paper deals with three fundamentally different concepts of self-lubricant coatings based on the transition metal dichalcogenides (TMD) and deposited by magnetron sputtering. The first two designs could be considered as traditional: the TMD films doped by carbon or nitrogen. The main attention is aimed at qualitative description of surface and sub-surface modification of the films as the result of the sliding process. Based on a thorough analysis of the worn surfaces, two features emerge: self-adaptability, where originally randomly oriented TMD phase becomes well oriented (i.e. with basal planes parallel to the surface), and limited role of carbon or nitrogen in the contact. The films doped with carbon are the best solution for humid environment, while those doped with nitrogen are ideal for use in dry environment or vacuum. The last concept deals with the combination of a hard TiN matrix deposited by reactive magnetron sputtering with fullerene-like TMD nanoclusters, which are directly injected into the growing TiN film. Despite the embryonic stage of the process development limiting in many ways the final properties of the film, the mechanical properties seem to be promising. The fullerene-like structure of TMD is well maintained and the composite hardness is relatively high compared to the competitive self-lubricant coating designs. On the other hand, the tribological tests did not show any effect of the embedded TMD nanoclusters in the sliding process.

Keywords: transition metal dichalcogenide; tribology; self-lubricant; fullerene-like particle; magnetron sputtering; tungsten disulphide

1. Introduction

Transition metal dichalcogenides (TMD) are compounds with unique and unusual properties based on the extreme degree of anisotropy of the layered crystal structures. TMD exists in the MX_2 form, where M = Mo, W, Nb and X = S, Se and Te. They are applied in various branches of science and technology, such as catalysts or fuel cells, and they are extensively used as solid lubricants. For most of tribological applications, the protection of the bulk material by thin films is a suitable method for improving the wear resistance. The most convenient method to prepare these films is magnetron sputtering; thus, all references hereinafter deals with coatings deposited by this method.

MoS_2 coating, the most known member of TMD family, was thoroughly analyzed in 80's and 90's. The first studies on the deposition of MoS_2 leaded usually to films with columnar morphologies with very high porosity and consequent very low values in hardness; the adhesion to the steel substrates was limited and the coatings deteriorated in the presence of humid air. Thus, their tribological behavior was unsuitable whenever high loads were applied to the sliding contact or tests were carried out in moisture containing atmospheres.

Other transition metal dichalcogenides have similar properties to those of molybdenum disulphide, but there are some important drawbacks which make them inappropriate for tribological applications. For example, it has been shown that pure niobium disulphides and diselenides exhibit poor lubrication properties due to their different electron structure in relation to MoS_2 [1], whereas the main drawback of sputtered tellurides is their strongly limited adhesion on steel substrates [2]. Nevertheless, there are studies showing that diselenides have improved resistance to water in relation to sulfides [3, 4].

Despite mentioned differences among pure TMD coatings, their common drawbacks are a very low load-bearing capacity, a low adhesion to the substrate and a detrimental effect of the air moisture in the tribological contact. There are many different possibilities to improve the tribological behavior of these coatings. One of the most successful ways is to deposit a composite material associating high strength materials with self-lubricants, i.e. doping of TMD film by other metals being titanium the most successful one [5,6,7,8,9].

Voevodin et al [10] brought a concept of nanocomposite structured coatings combining hard (WC) and self-lubricant (WS_2) phases embedded into amorphous carbon matrix. Similar concept was presented by Cavaleiro et al – W-S-C films deposited by magnetron sputtering [11,12,13]. The hardness and wear resistance of such coatings was significantly improved compared to that of pure WS_2; however, the coatings exhibited relatively high friction coefficient in humid air. As an alternative, WS_2 doped with nitrogen was developed [13,14].

Recently, a more complex study of TMD films doped with carbon was carried out. Three TMD materials were produced with carbon content varying between 25 and 70 at.%., namely W-S-C [15], Mo-Se-C [16] and W-Se-C [17] systems. The parameters of the deposition process were adapted in such way, that the film did not contain hard carbide nanograins. The films showed exceptionally low friction at humid air, negligible wear and, particularly, high load-bearing capacity.

Inorganic fullerene-like nanoparticles based on WS_2 (IF-WS_2) can be produced in large scale by chemical reactions consisting of the sulfidation in a reducing atmosphere at high temperatures of solid and vapour phase precursors based on W [18]. The tribological potential of such nanoparticles was clearly demonstrated [19,20,21]. We developed a method combining a nanocluster gun and a dc magnetron reactive sputtering equipment used for injecting preformed IF-WS_2 nanoclusters into the sputtered TiN matrix [22,23].

In this paper, we would like to summarize our work on TMD-based materials. We will present three different coating systems: TMD-C films with excellent frictional behavior in humid air, W-S-N optimized for the use in dry nitrogen and vacuum, and, finally, nanocomposite coating containing IF-WS_2 embedded into hard titanium nitride matrix.

2. Experimental details

TMD-C and W-S-N coatings were deposited on 100Cr6 and M2 polished steel samples with hardness close to 5 GPa and 9 GPa, respectively. The depositions were carried out in a radio-frequency magnetron sputtering Edwards ESM 100 unit, equipped with two cathodes (∅ = 100 mm). Prior to the depositions the substrates were sputter cleaned during 20 min by

establishing the plasma close to the substrates electrode. Immediately after, a Ti interlayer was deposited with an approximate thickness of 300 nm. In case of TMD-C, two deposition settings were used: i) one carbon sputtering target partly covered by TMD (WS_2 or $MoSe_2$) pellets placed preferentially in the eroded zone, and ii) TMD (WSe_2, MoS_2, or WS_2) and carbon targets used simultaneously. In case of carbon target covered by TMD, the dimensions of the pellets were 4.1×3.5×1.5 mm. The degree of target coverage determined the overall chemical composition of the sputtered film. The depositions were carried out with constant power density of 7.6 W/cm^2 in the carbon target. In case of two targets (TMD and C), the chemical composition was controlled by the power applied to each target. For W-S-N film, reactive sputtering from a WS_2 target in Ar/N_2 atmosphere was used.

The prototype system combining a dc magnetron sputtering equipment and the nanocluster gun to produce TiN-IF(WS_2) coatings was described in detail in previous papers [22,23]. The dc magnetron sputtering chamber has a pair of titanium targets (200x100 mm), placed directly opposite to each other, and a substrates holder positioned parallel to the symmetrical centre line of the two targets. The clusters gun consists mainly of two parts: (a) the cylindrical chamber and (b) the electromagnetic injector. A normal fuel injector (purchased from Bosch) was connected to the extreme side of the tube connecting the nanoclusters gun with the deposition chamber. The injector is normally closed and it opens to inject the pressurized gas when an electrical signal is applied to its solenoid coil. The injector has a disc-type outlet with four holes with diameter of about 150 µm (in total, 600 µm for the four holes). The frequency, the duration of the cycle and the repetition time can be varied through a dc pulse square wave generator. The IF–WS_2 nanospheres were synthesized employing WO_3 as precursors by a solid gas reaction [24,25]. Prior to injections, the IF–WS_2 nanospheres are kept inside the clusters chamber under different pressure (200 mbar – 2 bar) of argon gas. Three case fans are used inside the clusters chamber in order to facilitate the dispersion of the fullerene-like particles inside the clusters gun and to direct the flow close to the inlet of the injector. A Ti interlayer (approximately 100 nm thickness) was deposited between the nanocomposite and the substrate in order to improve its adhesion.

To evaluate the chemical composition of the films, an electron probe microanalysis was used. The hardness was determined by depth-sensing indentation technique with an applied load about 5 mN; the coatings deposited on M2 steel were used for these measurements.

The films structure was characterized by X-ray diffraction (XRD), microstructure by transmission electron microscopy (TEM), X-ray photoelectron spectroscopy (XPS), and Raman spectroscopy. Scanning electron microscopy (SEM) with energy dispersive X-ray spectrometry (EDS) was used to identify wear tracks features. Focused ion beam (FIB) was used to cut a slice through the wear track, which was then analyzed by TEM. Structural changes in the wear track were identified by Raman spectroscopy, the top surface composition gradient by Auger electron spectroscopy (AES). The tribological tests were carried out using a ball-on-disk tribometer with the 100Cr6 steel balls as the counterparts (diameter 6 mm). TMD-C and W-S-N films were tested in different ambient (dry nitrogen or air with a relative humidity of 40%) and temperatures (room to 400 ^{o}C). The tests were typically carried out with a load of 5 N; if the load was different, it is stated in the text. TiN films with WS_2 nanoclusters were tested only at room temperature in humid air.

TMD-C coatings were tested as well using SRV-OPTIMOL reciprocating testing equipment with 100Cr6 steel balls (diameter 10 mm) as sliding partners and the load in the range 20-1000 N; the frequency was 20Hz and the test duration 10 minutes (24 000 cycles). Different testing environments were used, such as humid air (30-40% relative humidity) or dry nitrogen.

3. Results and discussion

3.1 Transition metal dichalcogenides doped with carbon

We deposited four different TMD-C systems: two based on disulphides, W-S-C and Mo-S-C, and two based on diselenides, W-Se-C and Mo-Se-C. The carbon content was in the range 25 to 70 at.% for all systems except for Mo-S-C with maximum C content 55 at.%. Initial studies of W-S-C and Mo-Se-C systems [26,27,28,29] showed that the optimum carbon content for the tribological applications lays in relatively narrow range 40-55 at.%. Therefore, we repeated the deposition with conditions leading to approx. 50 at.% of carbon using large number of samples and carried out thorough coatings analysis together with extensive tribological testing including the wear track characterization.

Table 1 shows the main parameters of the TMD-C films. All deposited films are deficient in chalcogenide with respect to stoichiometric TMD target. However, molybdenum-based coatings posses relatively high Mo/S(Se) ratio close to ideal 1/2, while tungsten-based films are strongly substoichiometric with approx. 1/1 ratio. The excess of metal could be explained by a reaction of the oxygen and hydrogen from residual atmosphere with chalcogenides and metals, and by re-sputtering of light and weakly bonded chalcogenides atoms by neutral Ar species reflected at the target. Since tungsten is very heavy compared to molybdenum, the re-sputtering effect of the lighter element is significantly higher leading to lower amount of chalcogenides in the tungsten-based films. Selenium is less reactive and heavier compared to sulphur contributing to its higher content in the films.

The hardness of pure TMD (typically lower than 0.5 GPa) was increased by about one order of magnitude due to the addition of carbon. The coatings were dense and the porous columnar structure, typical for sputtered TMD films, disappeared, see **Fig. 1**. The TMD-C coating analyzes carried out by HR-TEM revealed a very specific microstructure with platelets of TMD phases embedded in the carbon matrix. TMD platelets consisting of single layers were separated from each other randomly oriented - more detailed description can be found in [15,16]. We did not observe any evidence of metal carbides in the films [30]. The microstructure observed by TEM corresponded to XRD pattern, which were almost identical for all TMD-C systems. The major peak at approx. 42° (2 theta) was highly asymmetric with a very long tail toward higher angles; it represents the turbostrating stacking of (10L) planes, L=0,1,2,..., which is observed when the TMD basal planes does not exceed several nanometers [25]. In some cases, a very weak peak was observed at approx. 67° corresponding to the (110) orientation of the TMD phase [30].

The tribological properties of all four systems exhibit remarkably similar features. The friction of such films does not follow Amonton's law, since the friction decreases with increased load. Such deviation is typical for pure TMD films, where the friction could be calculated by approximating the shear stress of solids at high pressures and the Hertzian model for contact pressure [24]. However, TMD-C does not follow this approximation (the friction linearly depends on $L^{1/3}$, L - load) and could be expressed by a power law fit $\mu \approx L^{b}$, where b is a constant depending on the TMD type and carbon content ($b > 0.4$). Typical example of the decrease of friction with load can be seen in **Fig. 2**; however, the calculations

were carried out from much larger number of measured points. The coatings were tested as well at SRV reciprocal pin-on-plate machine in order to estimate contact pressure limit. All systems withstood tests with 120 N (ideal Hertzian contact pressure 1.5-1.7 GPa), W-S-C coating was not worn through even after the measurement with a load of 1000 N (contact pressure 3.4 GPa). The friction again showed a decreasing tendency with increasing load; all films showed similar friction 0.06-0.07 at a load of 120 N.

AES chemical depth profiles showed the thickening of the surface TMD tribolayer when the contact pressure and/or the number of laps (i.e. test duration) was increased [15,16]. **Fig. 3** clearly demonstrates the absence of the carbon in the utmost surface of the wear track. In other words, the top layer is formed exclusively by TMD phase. However, the agglomeration of the TMD material in the contact zone could lead to the reduction of the friction coefficient providing that its basal planes are aligned parallel to the surface and no abundant oxidation occurs that can lead to strong bonding between them. The absence of oxygen in the top layer, confirmed by both Raman and AES, is an important factor facilitating the low friction. It should be pointed out that the top layer is fully oxygen free, while the as-deposited coating exhibit several at.% originating from the chamber residual atmosphere. Thin foils of the wear track surface were prepared by FIB technique and analyzed by TEM. The images revealed that TMD platelets on the top surface were fully aligned parallel to the wear track surface covering the most part of the zones which were analyzed. It was observed that the platelets were oriented even in the zone several tenths of nanometer below the wear track surface; however, the platelets were less ordered in such depth, i.e. the orientation of the basal planes parallel to the surface was still dominating, but not unique as in the utmost surface.

Only a limited number of the wear tracks (6 tracks - 6 different coatings) of the two systems (Mo-Se-C and W-S-C) were analyzed by AES and FIB/TEM; however, we have strong evidence that the behavior described above is typical for all the four systems. Raman spectroscopy is a sensitive tool to identify the structural changes on the surface of TMD-C films. We demonstrated [24,23] that the peaks of TMD were more intense and sharper in the wear track, when the surface and sub-surface reorientation occurred. On the other hand, the G and D bands of carbon, very intense for as-deposited coatings, strongly diminished when the analysis was done in the wear track. We showed that the ratio of TMD and carbon peaks increased with the load and the number of laps [28]. Therefore, the Raman spectroscopy confirmed the results of AES and FIB/TEM - re-orientation and grouping of TMD platelets

under sliding contact (sharpening of TMD peaks in Raman spectra) and absence of carbon in the top surface (significant decrease of the carbon peaks intensity). We applied Raman spectroscopy to many different samples and systems and all measurements corresponded with the results referred to above. Thus, the sliding process of TMD-C films at humid air exhibits low friction due to the following predominant factors: i) formation of an exclusive TMD layer in the contact; ii) optimum orientation of such layer allowing low friction and simultaneously improving the resistance to environmental attacks, and iii) sub-surface re-orientation of the TMD platelets, which can immediately take part in the sliding process when the top TMD layer is worn out.

The coating adaptation to the sliding process enhances the importance of a running-in process. Typical running-in represents the polishing of high asperities, which is followed by the steady-state wear. In such case, the initial friction is high with a tendency to increase, and after a relatively short time it stabilizes at the steady-state level (typically lower than that of running in). TMD-C films showed a different behavior. The initial high friction dropped quickly to a low level; however, it continued monotonically decreasing during several thousands of laps, where the stabilized friction level was reached. The length of such decrease depended on the sliding conditions being shorter for higher loads. The coating worn volume or wear track depth was directly related to the stage of running-in, since relatively high wear in the first thousands of laps decreased considerably with further development of the sliding process, see **Fig. 4**.

Based on our studies summarized above, we can now draw the scheme for optimum TMD-C coating performance in dry sliding in humid air:

- The contact pressure must be higher than a certain limit allowing the self-adaptation of the film;
- The presence of abrasive particles in the contact must be avoided, since they would destroy the thin TMD tribolayer;
- The initial roughness of the coating / substrate and the counterpart should be low.
- The coating and counterpart should be sliding in closed cycle with repetitive contact of identical coating and counterpart surfaces.

3.2 WS_2 coating doped with nitrogen

TMD-C films described in previous section exhibited low friction in dry air and dry nitrogen in the range 0.03-0.06 [31]. However, pure TMD could exhibit friction as low as 0.001 [32,33]. Therefore, we focused our attention to other system - tungsten disulphide doped with nitrogen, since preliminary tests showed its potential as a solid lubricant for dry sliding application in vacuum or dry nitrogen [14].

Sputtering from tungsten disulphide target in reactive Ar/N_2 atmosphere led to a film with a chemical composition 34 at.% of N, 12 at.% of O, 29 at.% of W and 25 at.% of S. XPS analysis showed the presence of W-N, W-S and W-O bonds with the later identified as tungsten trioxide. Therefore, considering the possible tungsten nitride phases and the presence of tungsten oxide, it seems that W/S ratio in W-S phase is close to stoichiometry of tungsten disulphide. W-N-S films thus posse much higher tungsten-to-sulphur ratio than transition metal-to-chalcogenide in case of the TMD-C films referred to above.

Despite the existence of tungsten disulphide and tungsten nitride, XRD spectra showed only very broad peaks typical for amorphous-like structures. **Fig. 5** depicts a TEM image of W-S-N film showing a completely amorphous-like and featureless film. The hardness of the coating was 7.7 GPa.

The tribological properties of W-S-N film at humid air were not satisfactory, particularly compared to TMD-C films. Despite the moderate wear rate, the friction was very unstable reaching a high average value, ~0.55. However, the tests in dry nitrogen showed an exceptional behavior. The friction was measured in two independent pin-on-disk devices to validate the results, since the measured friction force was close to the minimum limit of the equipments. The friction results produced by CSM Instruments pin-on-disc (100Cr6 ball with a diameter of 6 mm) exhibited average friction coefficient lower than 0.01 for the 5 N load and even negative friction -0.001 for the 55.8 N load, see **Fig. 6**. It should be pointed out that the highest possible systematic error of the equipment (particularly the error of calibration) was estimated to 0.003; therefore, we can conclude that the friction for higher load was lower than 0.003. In this case the nitrogen atmosphere was produced by flow of nitrogen into semi-closed pin-on-disc chamber and the nitrogen was thus always mixed with residual humid air giving up to 3% of air humidity. The tests were stopped after 5000 and 1000 laps for low and high load, respectively, in order to avoid the penetration of the film. To estimate the friction

behavior in the long-term test, pin-on-disc apparatus with full atmosphere control was used, where the sliding occurred in exclusive nitrogen atmosphere. Two loads were used, 5 N and 20 N; the 100Cr6 ball diameter was 10 mm. The test with 5 N was stopped after $0.8 \cdot 10^6$ laps with no evidence of the coating penetration and friction slightly increasing from 0.006 (end of running in) to 0.01 (end of the test). The second test with 20 N was stopped in the moment when the friction suddenly increased, i.e. when the coating was worn out. It took more than 2 million laps, as demonstrated in **Fig. 7**. Again, the friction dropped to the lowest level about 0.006 and then steadily increased to 0.015 in the moment when the coating was worn through.

The wear tracks of the film tested in humid air were analyzed by SEM revealing a smooth surface with small islands of thin adhered material. EDS did not detect any difference in the chemical composition in the wear track compared to the as deposited films; therefore, Raman spectroscopy was used to identify the wear track features. **Fig. 8** shows the Raman spectra taken inside the different zones of the wear track. The "free" surface, i.e. surface without evident adhered layer, showed peaks of tungsten disulphide and tungsten trioxide. The blue part exhibited only weak WS_2 peaks, while the black part is almost WS_2 free. Compared to the as deposited film, the absence of WS_2 peaks in the wear track produced by sliding in humid air is evident explaining the high friction. On the other hand, the wear track of the films tested in dry nitrogen showed almost identical spectra with those of as-deposited coatings; no traces of tungsten oxides were observed contrasting to the sharp and well defined WS_2 peaks. It seems probable that the sliding process in dry nitrogen was driven almost exclusively by the low-friction tribolayer of tungsten disulphide (see the Raman analyses of TMD-C films in previous section).

Finally, the W-S-N films were tested at elevated temperature, since the absence of air humidity was favorable for this type of material. **Fig. 9** shows friction curves at temperatures up to 400 ^{o}C. The friction coefficient at 100 and 200 ^{o}C was again very low close to detection limit of the equipment. The increase of the friction to 0.15 at 400 ^{o}C could be still considered as a promising result.

3.3 Sputtered TiN coatings with embedded WS_2 fullerene-like particles

The effect of the localized cluster injection was clearly visible - the film at the centre of the substrate, the place where the flow of injected particles was the highest, showed a grey color

and high surface roughness, while the rest of the coating exhibited features typical of stoichiometric TiN film. A mixture of TiN and Ti-O phases were identified in XRD spectra together with a strong peak at ~16.5º (in 2θ) corresponding to the (002) plane of the hexagonal WS_2 phase. Therefore, the IF-WS_2 nanoclusters were incorporated into TiN/Ti-O matrix. The TEM images further prove the presence of such nanoclusters with size in the range 50 - 150 nm (Fig. 10) identified by EDS analysis as WS_2. The surface coverage by IF-WS_2 nanoclusters was relatively high being estimated to be ~5%.

Chemical composition measured by EDS revealed a strong difference between the dark spot in the center of sample and the surrounding gold film. The later was identified as almost stoichiometric TiN with small contents of oxygen and no vestiges of W or S. Conversely, the dark spot showed Ti, W, S, O, and to some extent nitrogen. Therefore, it seems that the dark spot, where IF nanoclusters are present, was formed predominantly by Ti-O phases with only a minor part of TiN. These results are supported by XRD characterization. It seems that the injection process brought not only IF nanoclusters mixed with argon, but as well residual gases containing oxygen. The high affinity of Ti toward oxygen caused the immediate formation of Ti-O phases on the coating surface in the place where the nanoclusters were injected. The presence of residual oxygen flowing in could be explained by the relatively high ultimate vacuum pressure in the nanoclusters preparation chamber. This chamber was evacuated to only 10^{-2} Pa and then filled with Ar. In fact, the total amount of oxygen atoms was relatively low compared to the size of sputtering targets and chamber and under normal conditions would not dramatically increased the oxygen content in the film. However, when the flow was restricted to a very small area, the nitrogen was replaced by oxygen causing the formation of Ti-O phases. We believe that this issue could be avoided by increasing the distance between the injector tube and the substrate; however, the number of incorporated clusters would be much lower.

The presence of nanoclusters and Ti-O phases in the dark spot and predominantly TiN outside was confirmed by Raman spectroscopy. The spectra showed strong peaks positioned at 350 cm^{-1} and 420 cm^{-1} representing WS_2 and the peaks close to 440 and 610 cm^{-1} corresponding to TiO_2 in the rutile form [34]. Moreover, the peaks at 800 cm^{-1} (WO_3) revealed the partial oxidation of nanoclusters. Peaks of TiN (320 and 550 cm^{-1}) were observed only outside of the dark zone.

The surface roughness was strongly affected by the incorporation of nanoclusters. However, the size of nanoclusters was too small to explain the surface roughness with Rz above 2 µm, i.e. more than one order magnitude higher than the maximum size of individual or even agglomerated clusters. **Fig. 10** shows the TEM micrograph of the film cross-section in the dark zone. It is clearly seen that small nanocluster caused large voids. It should be pointed out that the experimental settings with sample positioned perpendicular to sputtering titanium target led to an inclined columnar growth and, consequently, strengthened the shadowing effect by nanoclusters. The presence of clusters is a key factor contributing to high roughness, since inclined sample position did not produce high roughness outside of the dark spot - TiN covered surface was still mirror-like. Obviously, the hardness in the dark zone was much lower (~7 GPa) compared to pure TiN film outside (~19 GPa).

The friction curves show similar features at two applied loads, 5 and 18 N. After short running in, the friction drops down to the lowest level and then steadily increases till the coating failure at approx. 1000 laps. Consequently, shorter tests with duration 500 laps were carried out. The depth of the wear track was then about one half of the initial coating thickness. The wear track was analyzed by Raman spectroscopy and the slice of the cross section of the top layer of the wear track was extracted by FIB and observed in TEM. A thin tribolayer with a thickness of 20-30 nm on the surface was observed; however, EDS revealed only Ti, Fe and O. This result was confirmed by Raman spectroscopy showing peaks exclusively related with rutile TiO2 and two iron oxides: peak at ~300 and 400 cm^{-1} corresponded to Fe_2O_3 and that at ~660 to cm^{-1} to Fe_3O_4 (**Fig. 11**). We can conclude that the presented coatings did not fulfill the criteria for self-lubricant films. The absence of tungsten disulphide in the contact, the high wear of the films and, particularly, the oxidation of the TiN matrix are issues to be addressed in further study.

4. Conclusions

We showed three different concepts of self-lubricant coatings: TMD-C and W-S-N films deposited by non-reactive and reactive magnetron sputtering, respectively, and TiN/IF-WS_2 prepared by a combination of magnetron sputtering of a titanium target and injection of IF-WS_2 nanoclusters. TMD-C coatings exhibited a very low friction in humid air due to their ability of self-adaptation, i.e. formation of a thin TMD layer in the contact and sub-surface re-

orientation of TMD platelets inside the carbon matrix. The tribological concept of such films is visualized in **Fig. 12**. W-S-N films showed extremely low friction in different moisture-free ambient - dry nitrogen or elevated temperature. In some cases, the friction was lower than 0.003. Finally, the self-lubricant film combining hard matrix and fullerene-like WS_2 nanoclusters was presented. The nanoclusters were successfully incorporated into the sputtered matrix; however, there were several drawbacks of our deposition method. The residual oxygen from cluster injector caused local oxidization of the TiN matrix. Moreover, the nanoclusters originated many voids in the grown coating due to shadowing effect. Consequently, the wear resistance of such films was not satisfactory. The analysis of the wear track did not reveal the presence of WS_2 in the contact; in other words, there was no benefit to incorporate IF-WS_2 nanoclusters for friction reduction.

Acknowledgements

This work was supported by the Czech Science Foundation through the project 108/10/0218. The authors acknowledge as well the Portuguese Science Foundation "Fundação para a Ciência e Tecnologia - FCT" for the project SFRH/BPD/34515/2006 funded under the program “Programa Operacional Factores de Competitividade (COMPETE)” from “Quadro de Referência Estratégico Nacional (QREN) co-participated by FEDER.

References

[1] P.D. Fleischauer, Thin Solid Films 154 (1987) 309

[2] E. Bermann, G. Melet, C. Muller, A. Simon-Vermot, Tribol. Int. 14 (1981) 329

[3] A.R. Lansdown, Molybdenum Disulphide Lubrication, Elsevier, 1999

[4] T. Kubart, T. Polcar, L. Kopecký, R. Novák, D. Nováková, Surf. Coat. Technol. 193 (2005) 230

[5] T.W. Scharf, A. Rajendran, R. Banerjee, F. Sequeda, Thin Solid Films 517 (2009) 5666

[6] D.G. Teer, Wear 251 (2001) 1068.

[7] A. Savan, M.C. Simmonds, Y. Huang, C.P. Constable, S. Creasey, Y. Gerbig, H. Haefke, D.B. Lewis, Thin Solid Films 489 (2005) 137.

[8] N.M. Renevier, V.C. Fox, D.G. Teer, J. Hampshire, Surf. Coat. Technol. 127 (2000) 24

[9] N.M. Renevier, J. Hamphire, V.C. Fox, J. Witts, T. Allen, D.G. Teer, Surf. Coat. Technol. 142–144 (2001) 67

[10] A.A. Voevodin, J.S. Zabinski, Thin Solid Films 370 (2000) 223

[11] A. Nossa, A. Cavaleiro, J. Mater. Res. 19 (2004) 2367

[12] A. Nossa, A. Cavaleiro, Surf. Coat. Technol. 163–164 (2003) 552.

[13] A. Nossa, A. Cavaleiro, N.J.M. Carvalho, B.J. Kooi, J.Th.M. De Hosson, Thin Solid Films 484 (2005) 389.

[14] A. Nossa, A. Cavaleiro, Tribol. Lett. 28 (2007) 59

[15] T. Polcar, M. Evaristo, A. Cavaleiro, Plasma Process. Polym. 6 (2009) 417

[16] T. Polcar, M. Evaristo, R. Colaço, C. Silviu Sandu, A. Cavaleiro, Acta Mater. 56 (2008) 5101

[17] M. Evaristo, T. Polcar, A. Cavaleiro, Plasma Process. Polym. 6 (2009) S92

[18] Y. Feldman, A. Zak, R. Popovitz-Biro, R. Tenne, Solid State Sci. 2 (2000) 663

[19] Y. Q. Zhu, T. Sekine, Y. H. Li, W.X. Wang, M. W. Fay, H. Edwards, P. D. Brown, N. Fleischer and R. Tenne, Adv. Mater. 17 (2005) 1500

[20] L. Rapoport, A. Moshkovich, V. Perfilyev, R. Tenne, Tribology Letters 28 (2007) 81

[21] L. Rapoport, N. Fleischer, R. Tenne, Adv. Mater. 15 (2003) 651

[22] D. Bharathi Mohan and A. Cavaleiro, Vacuum 83 (2009) 1257

[23] D. Bharathi Mohan, F. Svahn and A. Cavaleiro, Plasma Process. Polym. 6 (2009) S923

[24] Y. Feldman, A. Zak, R. Popovitz-Biro, R. Tenne, Solid State Sci. 2 (2000) 663

[25] R. E. Dinnebier, O. Gunnarsson, H. Brum, E. Koch, P.W. Stephens, A. Huq and M. Jansen, Science 296 (2002) 109

[26] T. Polcar, M. Evaristo, M. Stueber, A. Cavaleiro, Wear 266 (2009) 393-397

[27] T. Polcar, M. Evaristo, A. Cavaleiro, Wear 266 (2009) 388

[28] T. Polcar, M. Evaristo and A. Cavaleiro, Plasma Process. Polym. 4 (2007) S541

[29] T. Polcar, M. Evaristo, A. Cavaleiro, Vacuum 81 (2007) 1439

[30] T. Polcar, M. Evaristo, M. Stueber, A. Cavaleiro, Surf. Coat. Technol. 202 (2008) 2418

[31] M. Evaristo, T. Polcar, A. Cavaleiro, Int. J. Mech. Mater. Des. 4 (2008) 137

[32] D.R. Wheeler, Thin Solid Films 223 (1993) 78

[33] J. Moser, F. Levy, J. Mater. Res. 8 (1993) 206

[34] N. Fateh, G.A. Fontalvo, G. Gassner, C. Mitterer, Wear 262 (2007) 1152

Tables

Table 1 Typical properties of TMD-C coatings.

	Deposition rate (nm/min)	Chemical composition			Thickness (μm)	Hardness (GPa)
		W or Mo (at.%)	S or Se (at.%)	Carbon (at.%)		
W-S-C	35	24	22	54	2.1	9.2
Mo-S-C	7	17	28	55	1.2	3.9
W-Se-C	50	21	21	58	1.2	3.5
Mo-Se-C	36	17	31	51	2.6	2.9

Figure captions

Fig. 1 W-S-C (left) and Mo-S-C (right) coating cross-section observed by TEM.

Fig. 2 Friction coefficient of TMD-C films as a function of load (pin-on-disc).

Fig. 3 Representation of the depth profile measured by AES in the wear tracks. The wear track surface is on the left. The absence of carbon in the top layer is evident (dot line shows ratio of as-deposited coating).

Fig. 4 3D images of the wear tracks produced with increasing number of laps (pin-on-disc, load 5N, W-S-C film).

Fig. 5 TEM image showing featureless and amourphous-like W-S-N coating.

Fig. 6 Friction coefficient of W-S-N films in dry nitrogen as a function of the load. Note that the friction was in case of the higher load close to the detection limit of the equipment.

Fig. 7 Durability tests of W-S-N film in dry nitrogen (load 20 N, ball diameter 10 mm).

Fig. 8 Raman spectra taken in the wear track of a W-S-N coating sliding in humid air (1 - "blue" adhered layer, 2 - "black" adhered layer and 3 - "free" wear track) and spectra of the as-deposited coating (4).

Fig. 9 Evolution of the friction coefficient of W-S-N coating at elevated temperatures.

Fig. 10 TEM image of TiN/IF-WS_2 coating cross-section. Note the inclined columnar growth and IF-WS_2 particles causing voids.

Fig. 11 Raman spectra taken from the TiN/IF-WS_2 coating (left) and from the wear track surface (right). The later shows no vestiges of peaks related to tungsten disulphide at 350 and 420 cm^{-1}.

Fig. 12 Summarized tribological design of TMD-C films.

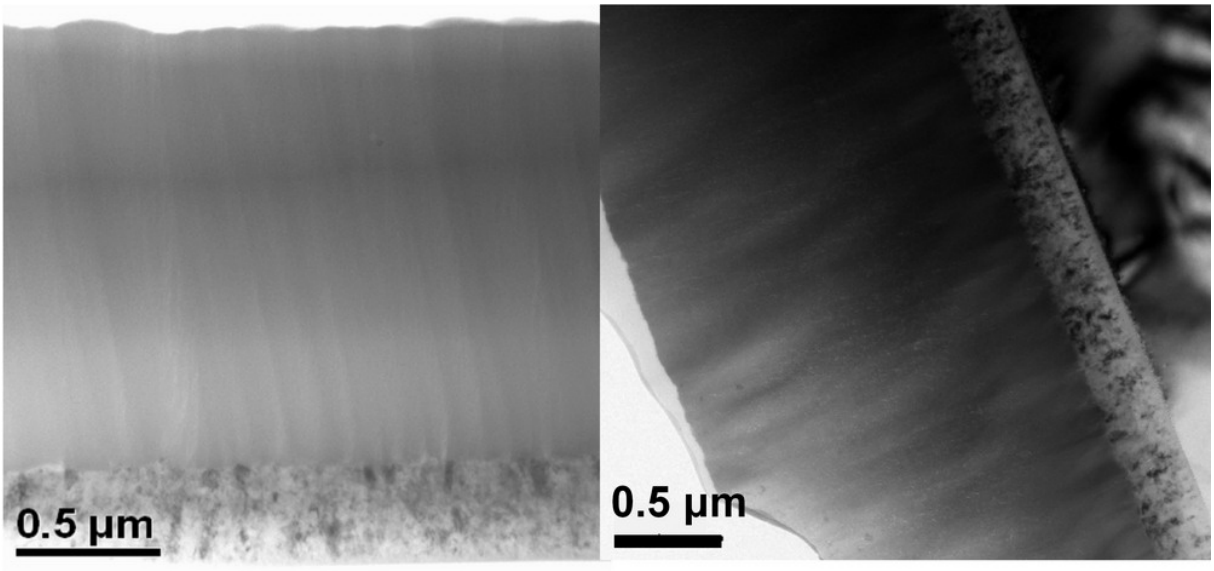

Fig. 1

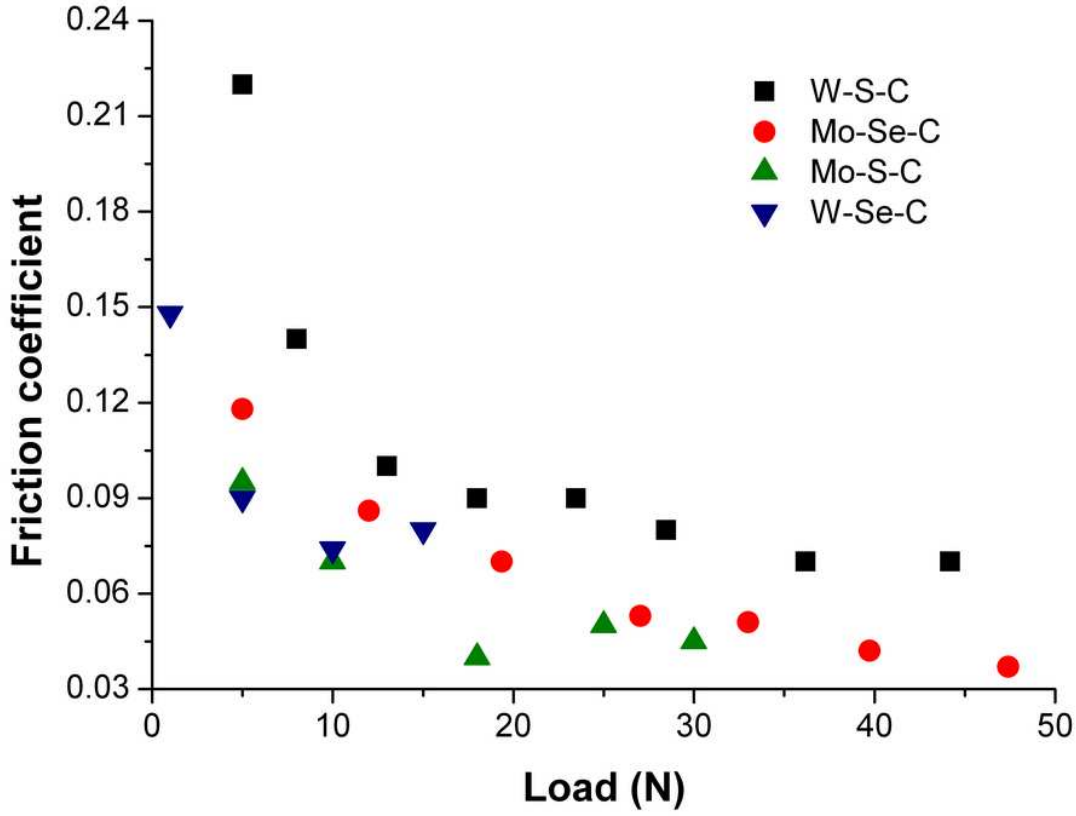

Fig. 2

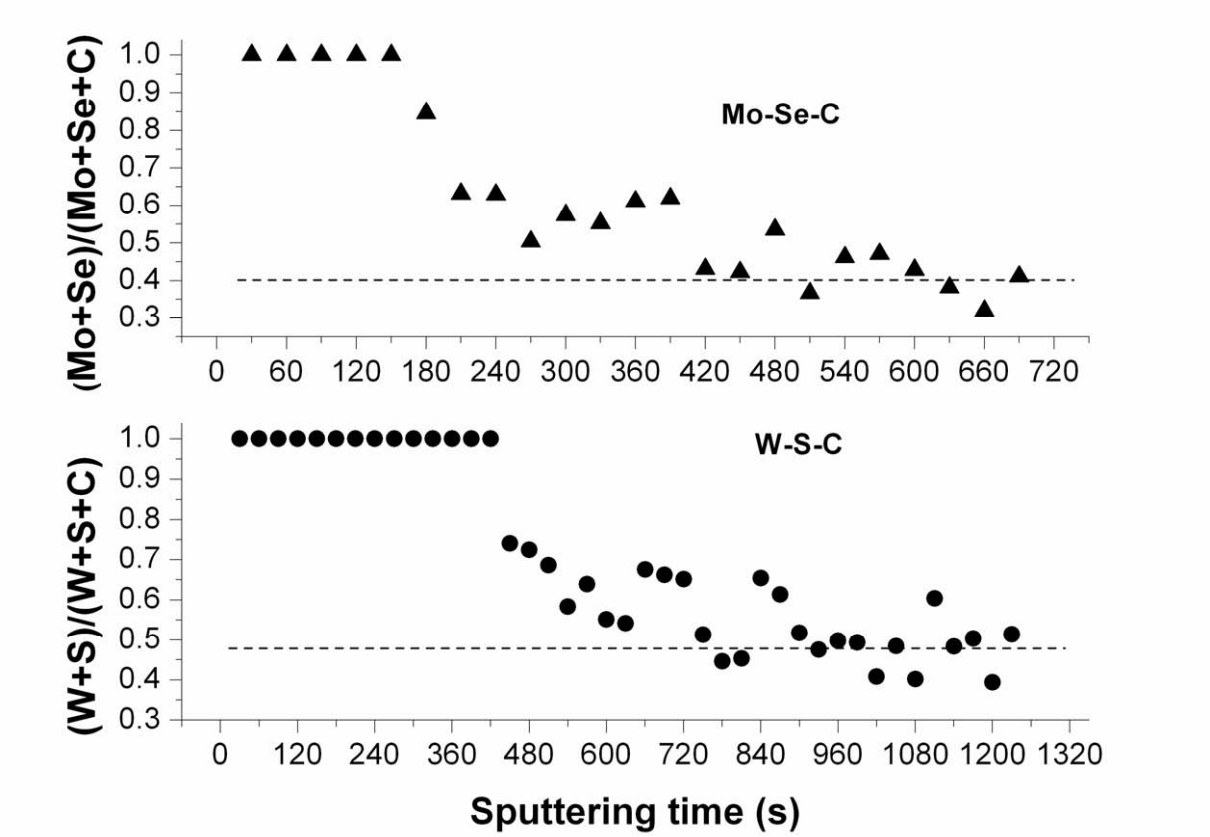

Fig. 3

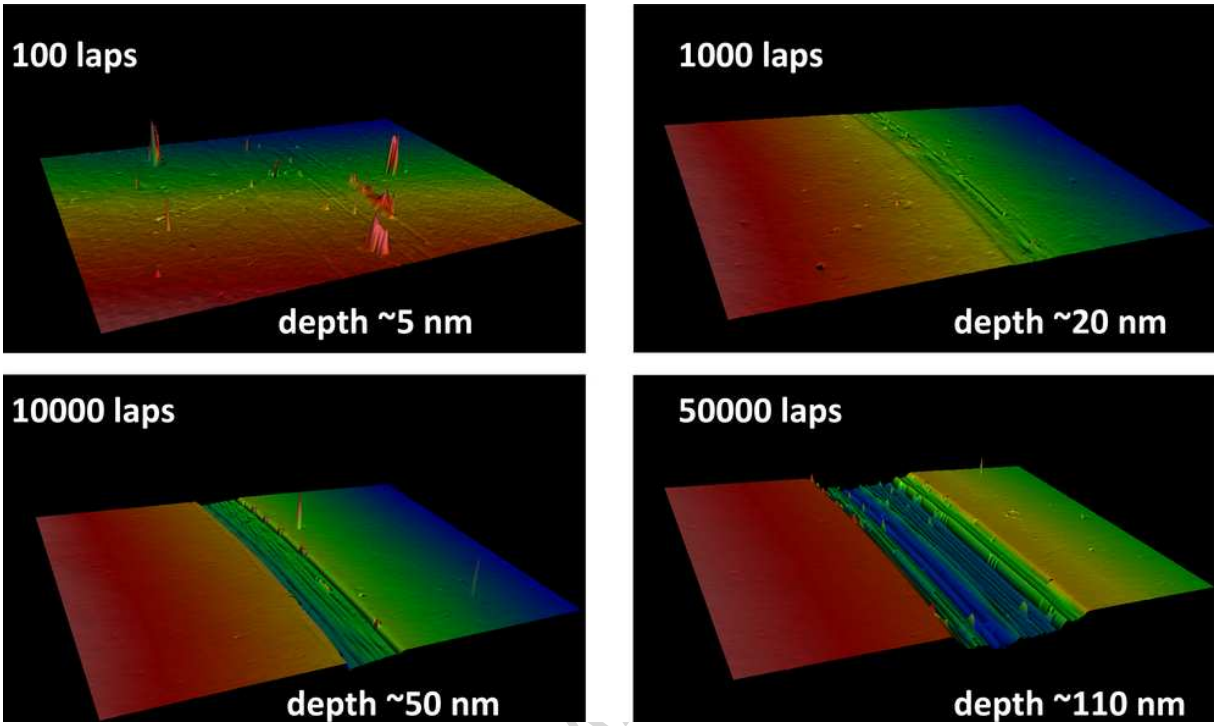

Fig. 4

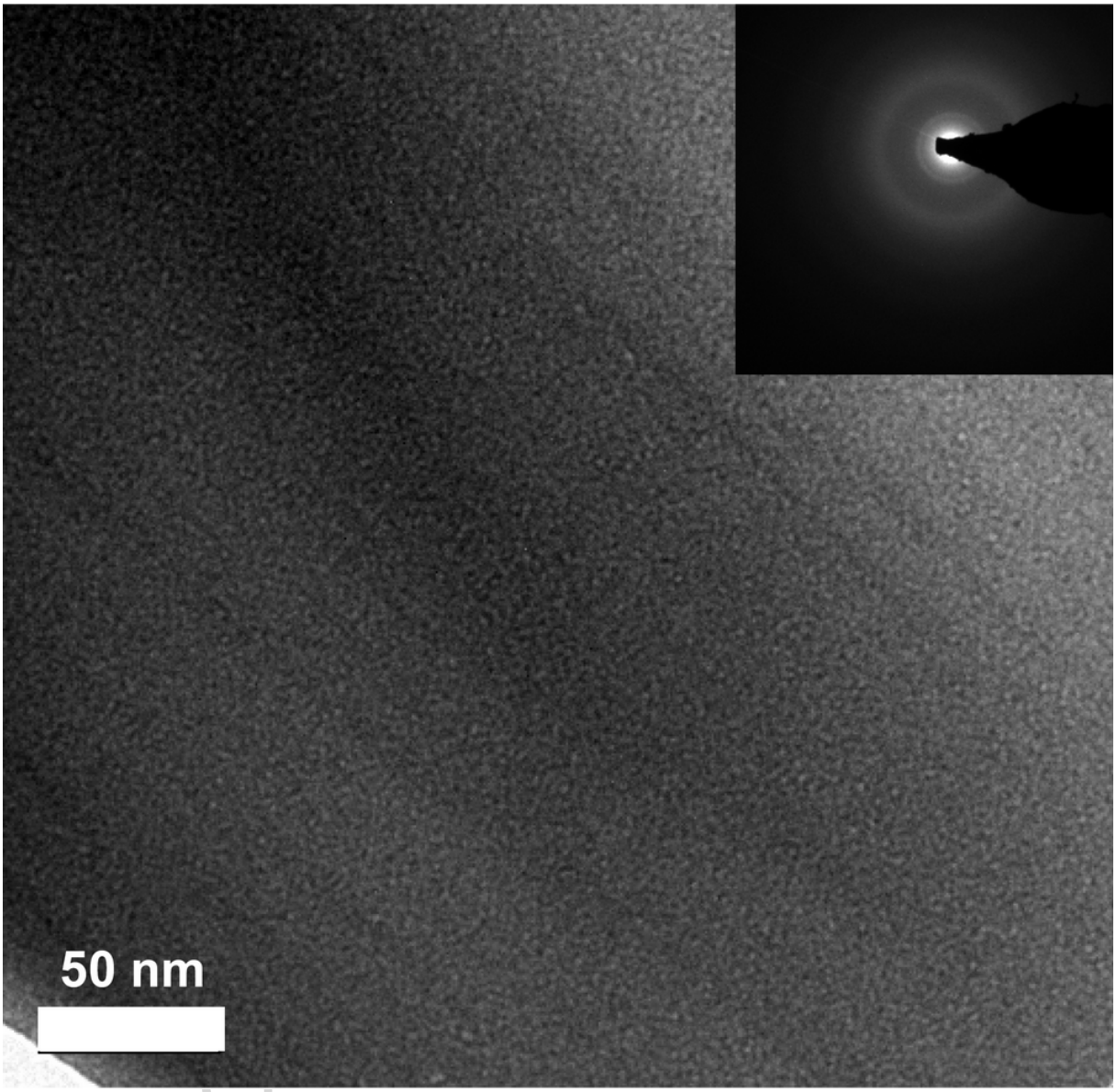

Fig. 5

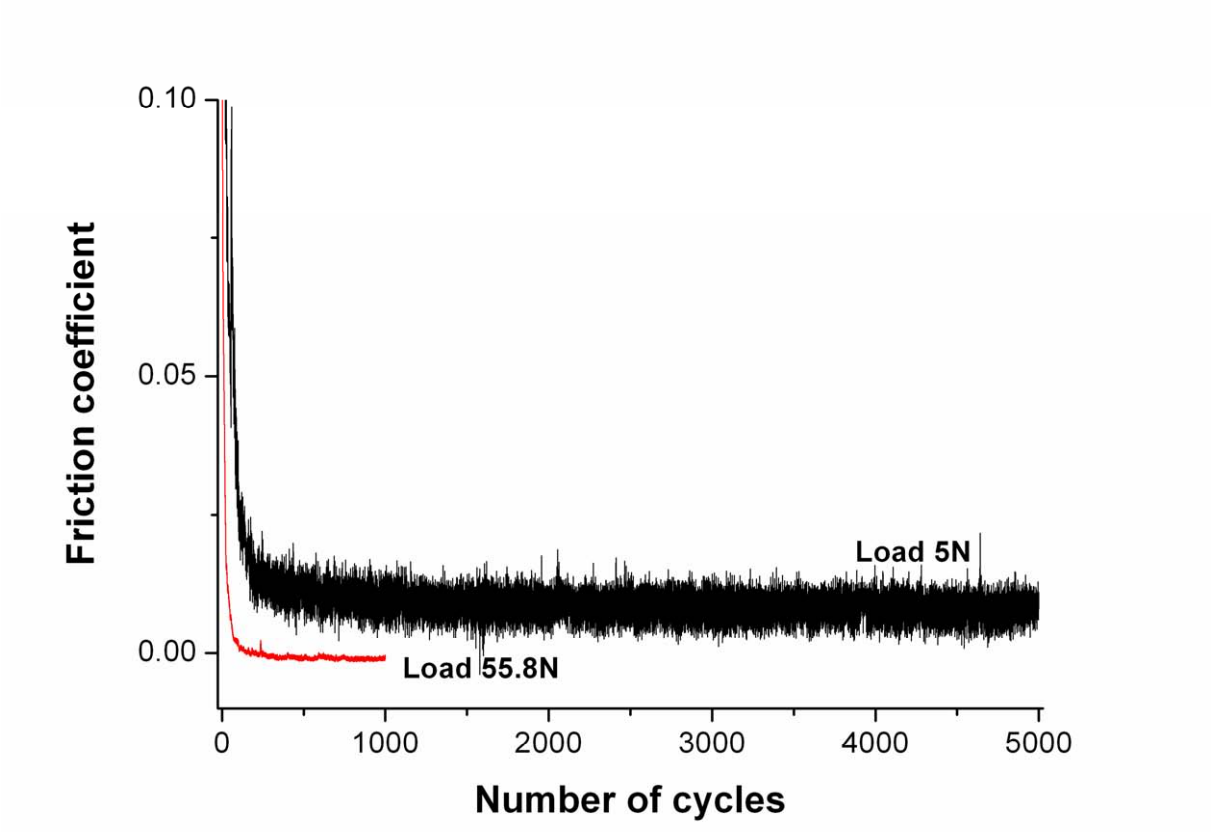

Fig. 6

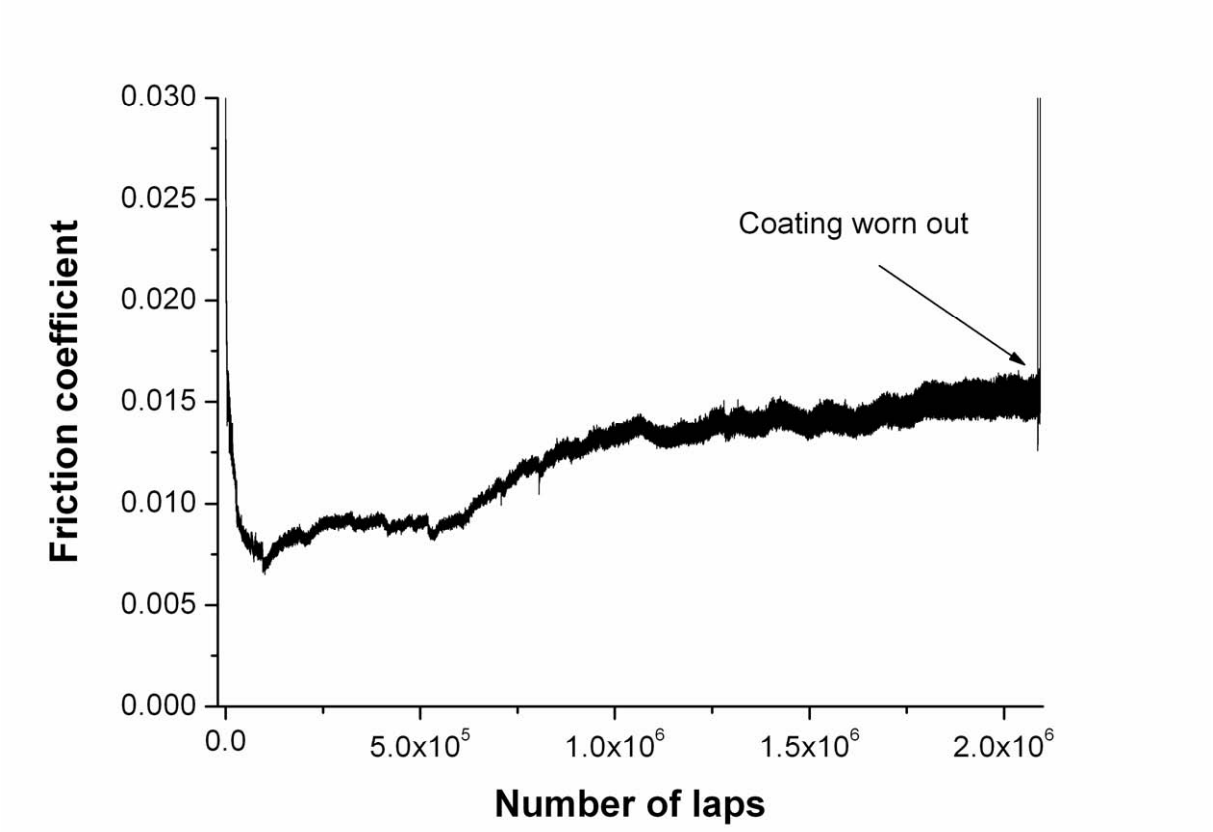

Fig. 7

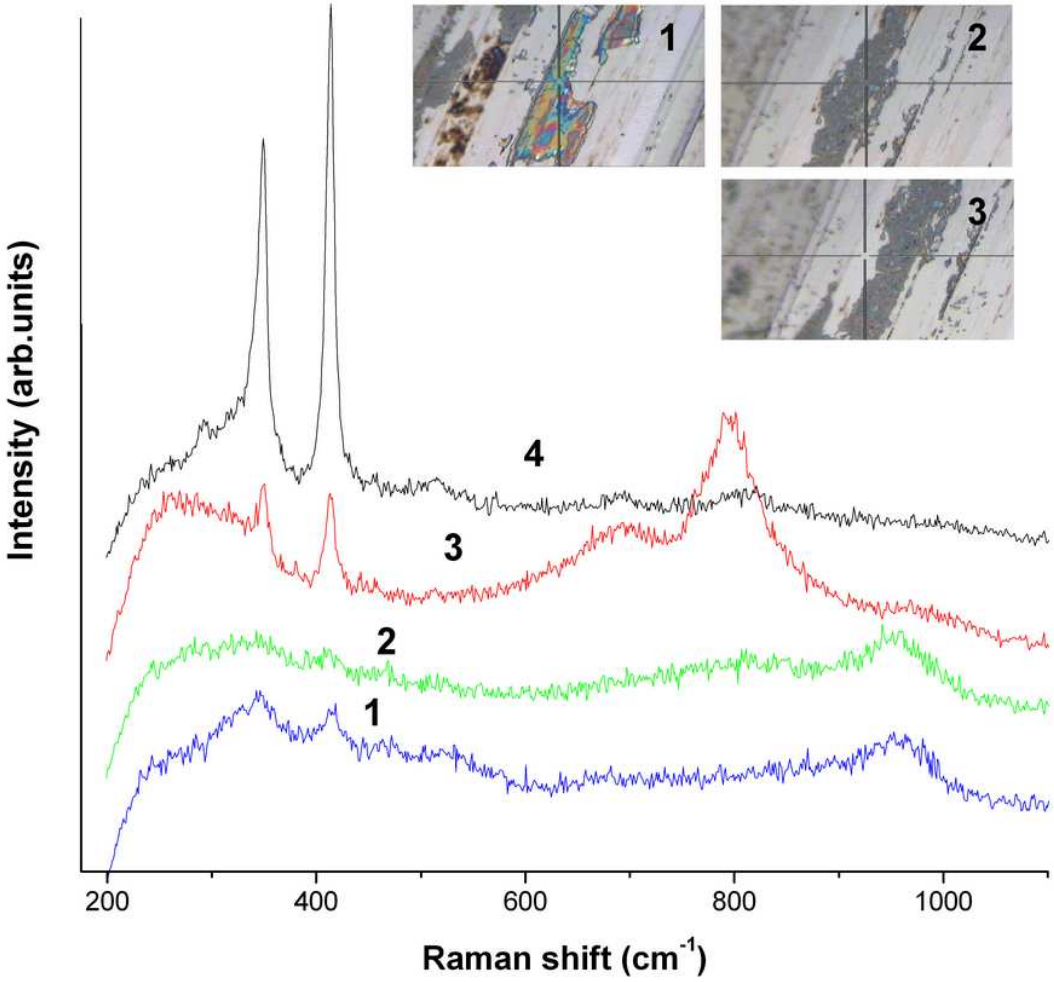

Fig. 8

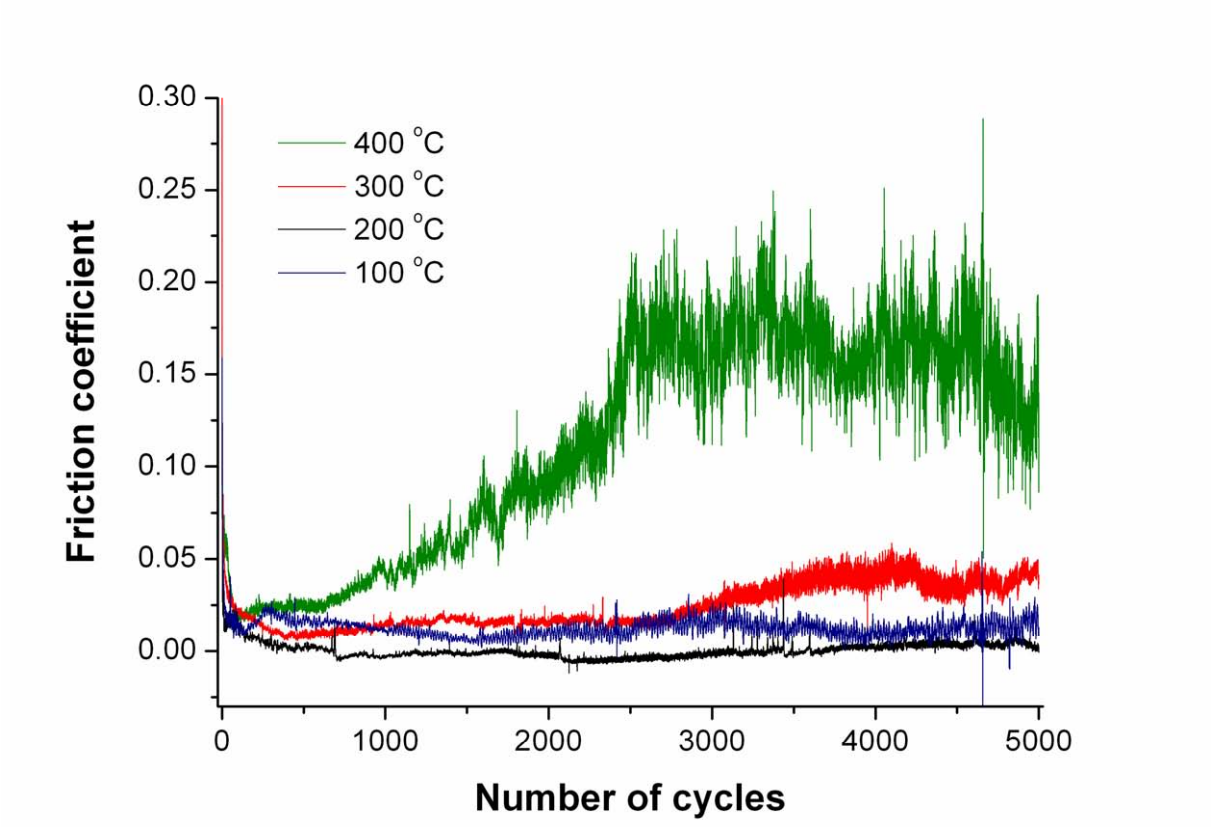

Fig. 9

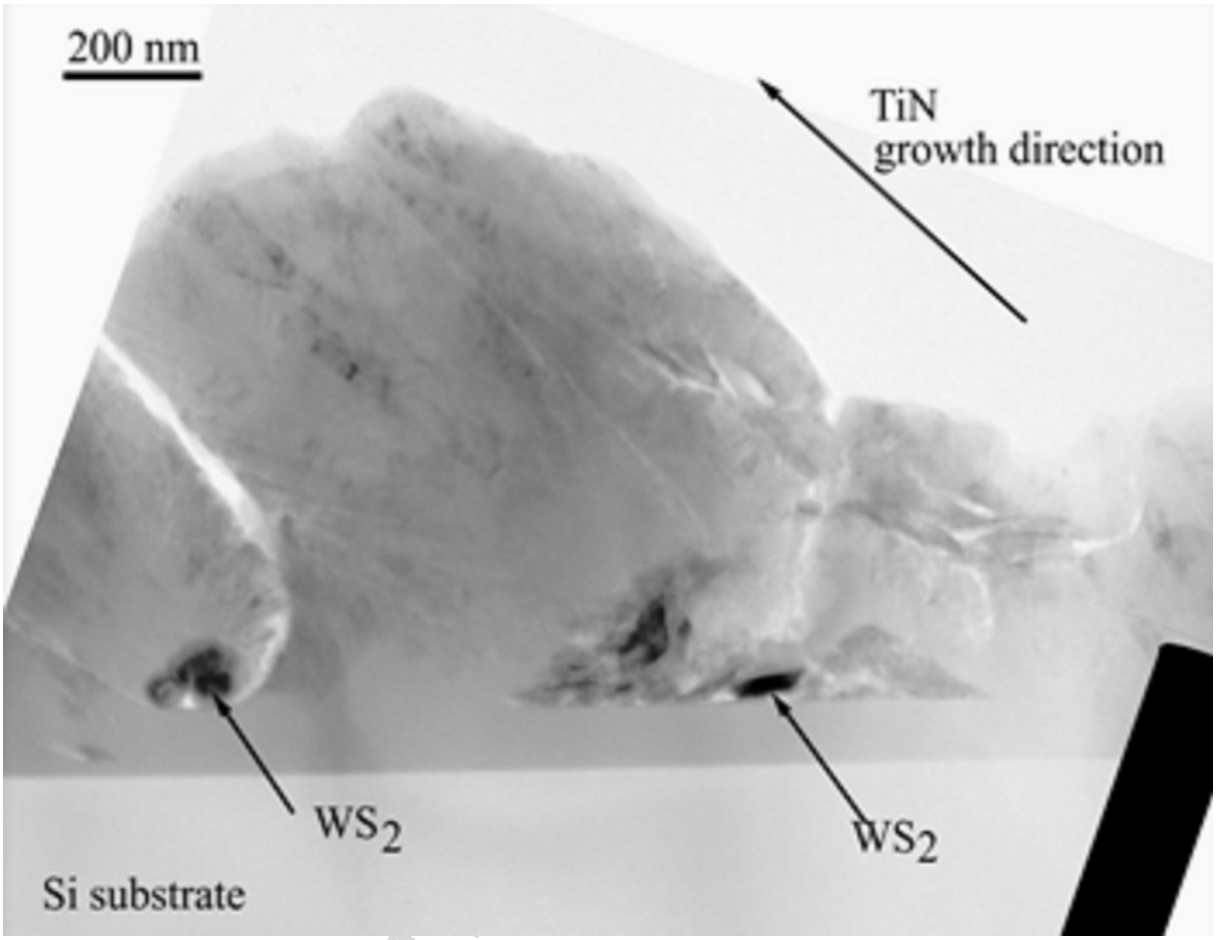

Fig. 10

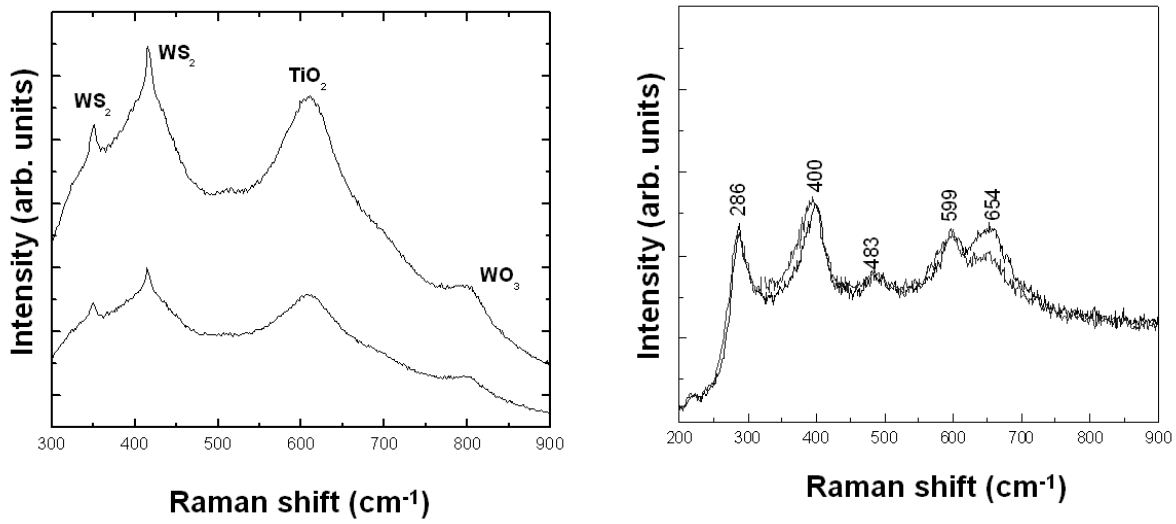

Fig. 11

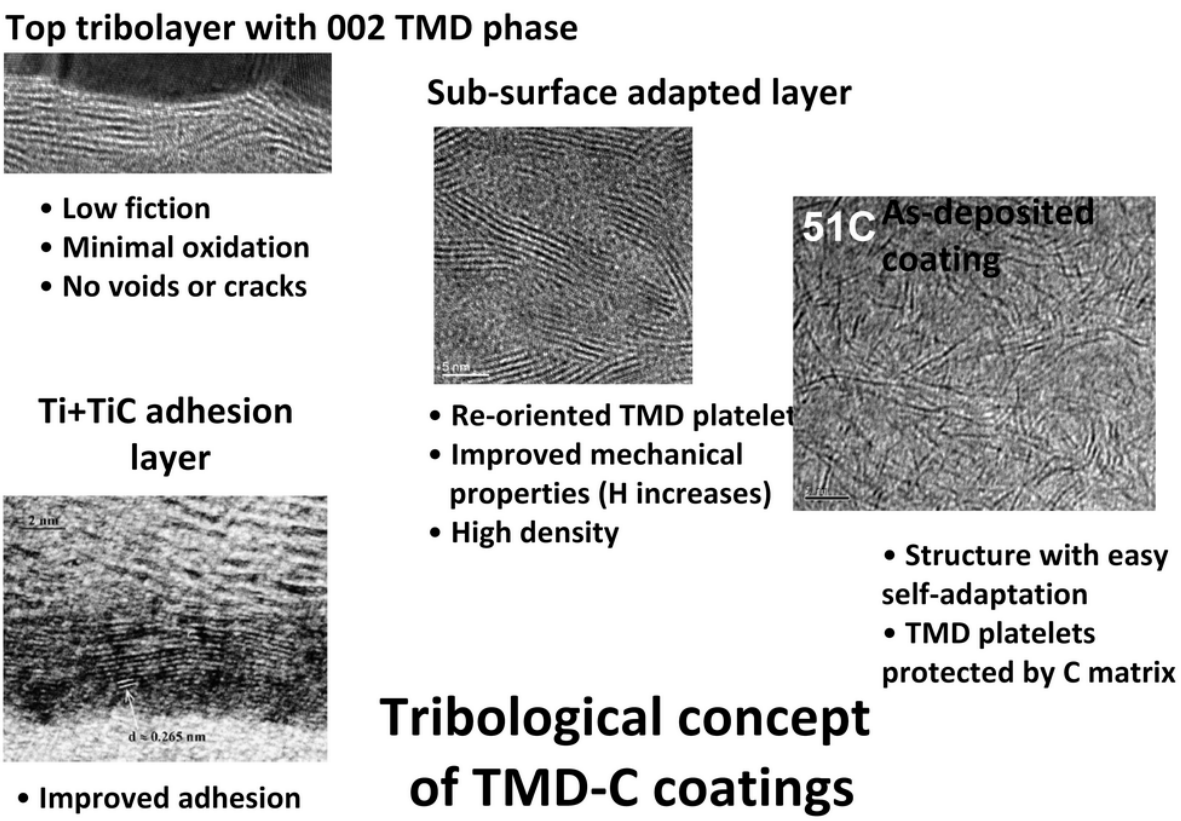

Fig. 12